Plasma blob formation by ion kinetic Kelvin–Helmholtz and interchange instabilities

2014 Plasma Phys. Control. Fusion 56 035012

(http://iopscience.iop.org/0741-3335/56/3/035012)

IOP Publishing Plasma Physics and Controlled Fusion

Plasma Phys. Control. Fusion **56** (2014) 035012 (9pp) doi:10.1088/0741-3335/56/3/035012

Plasma blob formation by ion kinetic Kelvin–Helmholtz and interchange instabilities

P W Gingell[1,2], S C Chapman[1,3,4] and R O Dendy[1,5]

[1] Centre for Fusion, Space and Astrophysics, Department of Physics, University of Warwick, Coventry, CV4 7AL, UK
[2] School of Physics and Astronomy, Queen Mary University of London, London, E1 4NS, UK
[3] MPIPKS, Nöthnitzer Straße 38, 01187 Dresden, Germany
[4] Dept. of Mathematics and Statistics, University of Tromsø, N-9019 Tromsø, Norway
[5] Euratom/CCFE Fusion Association, Culham Science Centre, Abingdon, OX14 3DB, UK

E-mail: p.w.gingell@qmul.ac.uk

Received 22 November 2013, revised 13 January 2014
Accepted for publication 27 January 2014
Published 18 February 2014

Abstract

The near-edge region of a tokamak is observed to generate radially propagating, coherent filamentary structures ('blobs'), which transport particles and heat from the confined region and across the scrape-off layer. The distribution of blob sizes may include a currently unresolvable population with radii comparable to the ion gyro-radius. Here, we conduct large-scale numerical simulations to study mechanisms for the creation of ion gyro-scale blobs via the ion kinetic Kelvin–Helmholtz and interchange instabilities, using a hybrid (kinetic ion, fluid electron) model. We present statistics of the sizes of blobs created by these instabilities, and radial particle displacement data. We find that ion gyro-scale blobs constitute a significant portion of the blob population, and that an increase in ion gyro-radius results in an increase in radial transport. Results are contrasted for pure proton plasmas and for 50 : 50 deuterium–tritium mix, relevant to burning plasmas. We conclude that ion kinetic physics plays a significant role in the transport of energy and particles by ion gyro-scale blobs in the near-edge region of low-field tokamaks.

Keywords: plasma blobs, Kelvin–Helmholtz instability, interchange instability, tokamaks, hybrid simulations

(Some figures may appear in colour only in the online journal)

1. Introduction

Turbulent fluctuations observed in the near-edge, confined region of tokamaks [1, 2] arise as a result of the saturation of the drift and interchange instabilities at the outboard side of the torus, which are driven by magnetic curvature and pressure gradients perpendicular to the magnetic field direction. Fluctuations of density, electron temperature and potential have been observed with amplitude 5–100% of the background, with smaller fluctuations in the magnetic field [3]. Intermittent detachment of coherent structures emerging from the turbulence, with subsequent radial transport due to charge polarization, forms the classical model of plasma blob creation and propagation in the near-edge region of tokamaks [4]. Populations of these structures have been reported for several tokamaks [5–9], and may account for as much as 50% of particle transport across the scrape-off layer (SOL) towards the vessel wall [5]. The transport of particles and heat by blob populations is of critical importance to future experiments [10], and hence a more complete understanding of the underlying physics is desirable.

Blob creation phenomenology differs between three important regimes for poloidal flow: no shear, weak shear and strong shear [11]. These sheared flows arise from momentum transport by Reynold's stress and blobs, or by transport barrier formation. With no shear present, the curvature driven

interchange instability results in the development of radial streamers [12]. These may become charge polarized and propagate in the same manner as blobs. In the low-confinement L-mode with weak shear, the dominant mechanism for blob creation is again the curvature driven interchange instability [13]. However, in this case the weak shear can result in the breakup of radial streamers into detached blobs, on the condition that the shearing time is shorter than the radial convection time [13]. Similarly, the action of shear flow can cause larger blobs to split into smaller ones. In these cases of weak or no shear, blobs are preferentially generated in the region of maximum pressure gradient [7]. The position of that region is dependent upon the density [14], and for sufficiently high densities, blobs can be preferentially generated inside the separatrix [15]. The appearance of blobs within the last closed flux surface (LCFS) of L-mode plasmas means that the gradients in these closed field line regions are sufficient to instigate blob creation.

In the high-confinement H-mode, zonal flows with strong shear boundaries are self-generated by turbulence. These strong shears suppress the transport of blobs compared to that found in L-mode plasmas, either by trapping them in the shear layer [16] or by blobs being torn apart by the shear itself. Despite this suppression, there is experimental evidence to suggest that the strong shear boundary can play a role in blob creation in toroidal plasmas such as JET [17], ASDEX-U [8] and TORPEX [18], where blobs are born in the sheared flow layer.

In principle blob diameters extend down to ion gyro-scales, and ion particle dynamics play an important role in blob creation, transport and evolution at these scales. This invites a kinetic numerical study. However, the ion gyro-scales of interest here represent an intermediate level of approximation between fully kinetic treatments and previous studies in the fluid regime. On these intermediate scales, it is necessary to capture the gyration of ions around magnetic field lines, while the gyration of electrons can be neglected. Hence a hybrid model is required in which ions are treated kinetically, and electrons as a fluid. A hybrid model has numerous advantages which apply directly to the results presented here. These include capture of the nonlinear interaction between ion gyration and plasma inhomogeneity; cross-scale coupling between ion gyro-scale kinetic modes and fluid MHD-like modes; resolution of phenomena on much shorter timescales than fluid models; and the ability to study non-Gaussian ion velocity distributions, while incorporating several distinct ion populations.

Previous investigations of the physics of ion gyro-scale blobs have demonstrated, first, that ion gyro-scale blobs develop significant asymmetries in their evolution compared with larger scale, fluid blobs [19, 20] and, second, that these ion gyro-scale blobs can heat the plasma at a faster rate than their larger counterparts [21]. In order to properly assess the consequences of gyro-scale blobs for tokamak plasmas, and make comparisons with those at fluid scales, we need to know the statistics of blob creation on ion gyro-scales. Since observations on these scales using contemporary diagnostics are difficult, we explore this regime by means of large-scale numerical simulation.

In this paper, we simulate blob creation on the ion gyro-scale using a hybrid code comprising kinetic ions and fluid electrons. The initial and boundary conditions chosen represent shear boundaries [22] and density gradients in the near-edge, confined region, for which the Kelvin–Helmholtz (K–H) and interchange instabilities are the principal sources of structure formation. The statistics of blob creation and particle displacement are discussed: we find that ion gyro-scale blobs can constitute a substantial portion of the blob population; and that increasing the ion gyro-radius relative to the width of the region of flow shear increases the associated particle transport.

2. Simulations

A detailed description of the general hybrid approximation can be found in [23]. The hybrid description treats ions kinetically as particles whose trajectories in the full six-dimensional (6D) phase space result from the Lorentz force arising from three-dimensional (3D) vector $\boldsymbol{E}$ and $\boldsymbol{B}$ fields. Electromagnetic fields are evolved self-consistently from Maxwell's equations and Ohm's law in the low-frequency Darwin limit [26]. The model assumptions are inertia-less electrons; $\boldsymbol{\nabla}\cdot\boldsymbol{E}$ negligible on length scales of interest, implying charge neutrality such that $en_\mathrm{e} = \sum_i q_i n_i$; collisionless plasma; and an ideal, isothermal electron fluid $\nabla\cdot\underline{\underline{P_\mathrm{e}}} = \nabla p_\mathrm{e} = kT_\mathrm{e}\nabla n_\mathrm{e}$. The full 3D $\boldsymbol{E}$, $\boldsymbol{B}$ and $\boldsymbol{J}$ vector fields are advanced with second-order accuracy on a two-dimensional (2D) grid in space (x, y) and in time. Particle positions are updated in two-dimensions in configuration space and three-dimensions in velocity space, and are therefore tracked in a five-dimensional (5D) phase space (x, y, v_x, v_y, v_z). No spatial variation of fields or particles is considered in the z-direction. Hence, we present simulations with '2D3V' geometry.

The hybrid code updates the magnetic field using Faraday's law, and the electric field using the electron fluid momentum equation:

$$n_\mathrm{e}m_\mathrm{e}\frac{\mathrm{d}\boldsymbol{v}_\mathrm{e}}{\mathrm{d}t} = -en_\mathrm{e}(\boldsymbol{E}+\boldsymbol{v}_\mathrm{e}\times\boldsymbol{B}) - \nabla\cdot\underline{\underline{P_\mathrm{e}}}. \qquad (1)$$

Here m_e is the electron mass, n_e is the electron fluid number density, $\boldsymbol{v}_\mathrm{e}$ is the electron fluid velocity, $\underline{\underline{P_\mathrm{e}}}$ is the electron pressure tensor, and $\boldsymbol{E}$ and $\boldsymbol{B}$ are the electric and magnetic fields respectively. Under the above assumptions, and neglecting resistive coupling between the electrons and the ion particle species, this equation can be written as an Ohm's law with the following form:

$$\boldsymbol{E} = -\frac{1}{en_\mathrm{e}}\left(kT_\mathrm{e}\nabla n_\mathrm{e} + \frac{\nabla B^2}{2\mu_0} - \frac{(\boldsymbol{B}\cdot\nabla)\,\boldsymbol{B}}{\mu_0} + \boldsymbol{J}_\mathrm{i}\times\boldsymbol{B}\right), \qquad (2)$$

where T_e is the electron fluid temperature, and $\boldsymbol{J}_\mathrm{i}$ is the ion current density. The hybrid approach and chosen geometry allow for the propagation of magnetoacoustic waves and the full resolution of ion gyration in the simulation plane.

The 2D grid is chosen with 960 cells in the x-direction and 240 cells in the y-direction, with cell size $\Delta x = 3.75\times10^{-3}\,\mathrm{m} = 0.4\rho_\mathrm{p}$, where ρ_p denotes the mean proton gyro-radius. The time step is determined by the Courant–Friedrichs–Lewy condition and is on the order of 10^5 time

Table 1. Physical and numerical parameters for simulations presented in this paper.

Parameter	
Background proton gyro-radius, ρ_p	8×10^{-3} m
Background proton gyro-period, t_{Ω_p}	1.6×10^{-7} s
Spatial resolution, Δx, Δy	$0.4\rho_p$
Total particles	2×10^7
Background magnetic field, $\boldsymbol{B}_0$	0.4 T
Background number density, n_0	10^{19} m^{-3}
Temperature, T_0	4×10^6 K
Alfvén speed, v_A	2.8×10^6 ms^{-1}
Sound speed, c_s	2.3×10^5 ms^{-1}
Background plasma beta, β	0.01
Electron Debye length, λ_D	4.4×10^{-5} m

steps per ion gyro-period. We use sufficient particles per cell to fully represent the ion velocity distribution and a typical simulation employs 2×10^7 total computational particles, or roughly 100 particles per cell. The $\pm x$ boundaries are periodic, and the $\pm y$ boundaries are open with a particle source at background conditions defined below.

Background parameters, chosen to be representative of conditions towards the edge of a low-field tokamak, are as follows: $n_0 = 10^{19}$ m^{-3}, $T_i = T_e = 4 \times 10^6$ K, $B_0 = 0.4$ T. Derived parameters are given in table 1. Several initial conditions are discussed, which lead to the growth of the interchange or K–H instabilities separately and in combination, for both proton plasmas and, for cases more relevant to burning plasmas, a 50 : 50 deuterium–tritium mix.

We simulate a boundary region internal to the plasma. A density gradient is set up at $y = 0$, with width a and maximum and minimum densities $n_{bot} = 4n_0$ and $n_{top} = n_0$ respectively, thereby initializing the simulation with a pressure gradient to drive the interchange instability. Some simulations also include a velocity shear boundary at $y = 0$, with $u_{bot} = -0.02v_A$ and $u_{top} = 0.02v_A$. The initial width a of both the density gradient and shear boundary is equal to the cell size Δx. The plasma is initially homogeneous in the (x, y) plane in both temperature and magnetic field, with background magnetic field $\boldsymbol{B}_0 = (0, 0, B_0)$ initialized perpendicular to both the plane of the simulation and the background flows. Consequently, there is no magnetic shear present in the initial conditions. For the simulations presented here, fluctuations in B_z grow with maximum amplitude on the order of 1% of the background field. Given the 2D3V simulation geometry, there are no gradients of the $\boldsymbol{B}$ field in the z-direction. A diagram of this geometry is given in figure 1.

3. Results

The results presented here focus on three aspects of the creation of blobs and the evolution of the boundary layer in the presence of the K–H and interchange instabilities. First, we examine the dynamics of the evolving internal plasma boundary. Second, we discuss the creation of coherent structures by these instabilities in terms of the distribution of structure sizes. Finally, we discuss the statistics of particle displacement perpendicular to the boundaries.

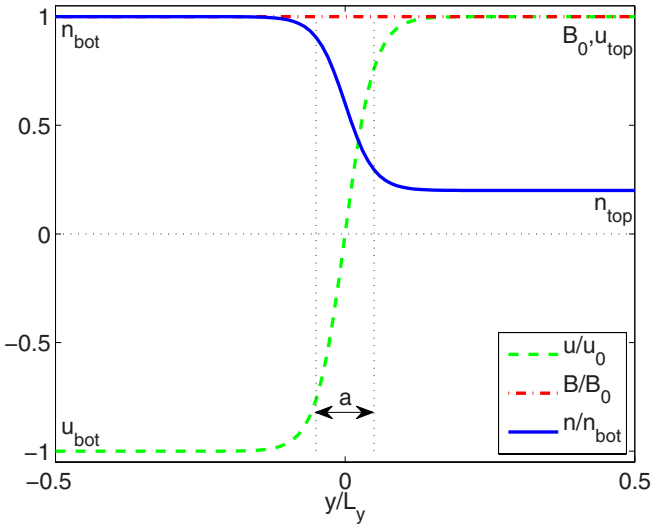

Figure 1. Initial conditions for the simulations presented in this paper. The initial velocities $u_{top,bot}$ are directed in the $\pm x$ directions, parallel to the boundary layer. The background magnetic field B_0 is directed in the z direction, perpendicular to the plane of the simulation domain and the background flows.

3.1. Dynamics of the internal plasma boundary

The time evolution of the number density of a simulation of a proton plasma with $n_{top} = n_0$, $n_{bot} = 4n_0$ and $u_{top/bot} = 0$ is shown in figure 2. In this scenario, we observe separation of populations of ions from their initial populations. Fingers of high-density plasma penetrate the $y > 0$ region originally occupied by low-density plasma. These finger-like structures, which have scale lengths on the order of the boundary width, are on spatio-temporal scales which are characteristic of the interchange instability [24]. As seen in figure 2, perturbations at the boundary layer extend in the y-direction from $122t_\Omega$, with separation of blob-like, coherent structures from the fingers beginning at approximately $180t_\Omega$. Meanwhile holes of low-density plasma arise in the $y < 0$ region. Additionally, these structures are seen to propagate in the $\pm y$ direction by virtue of the velocity imparted to these populations by the interchange instability. Hence, we can conclude that the interchange instability can lead to the formation of radially propagating blobs in the plasma region adjacent to the density interface. The amplitude of magnetic fluctuations is less than 1% of the background field over the full simulation domain, and we do not observe a changing magnetic topology via reconnection. Our simulations thus demonstrate that it is not necessary for the plasma and magnetic field conditions required for magnetic reconnection to exist in order for blob detachment to occur, once ion kinetics are fully incorporated in the physical model. Importantly for the interpretation of tokamak edge plasma observations, density blob detachment does not need to incorporate magnetic flux tube detachment by reconnection of magnetic surfaces: the blob birth process can be reconnectionless.

We now examine a case for which both interchange and K–H instabilities are active, by including in our initial conditions a velocity shear boundary at $y = 0$ with $u_{top/bot} = \pm 0.02v_A$. The evolution of the number density for these

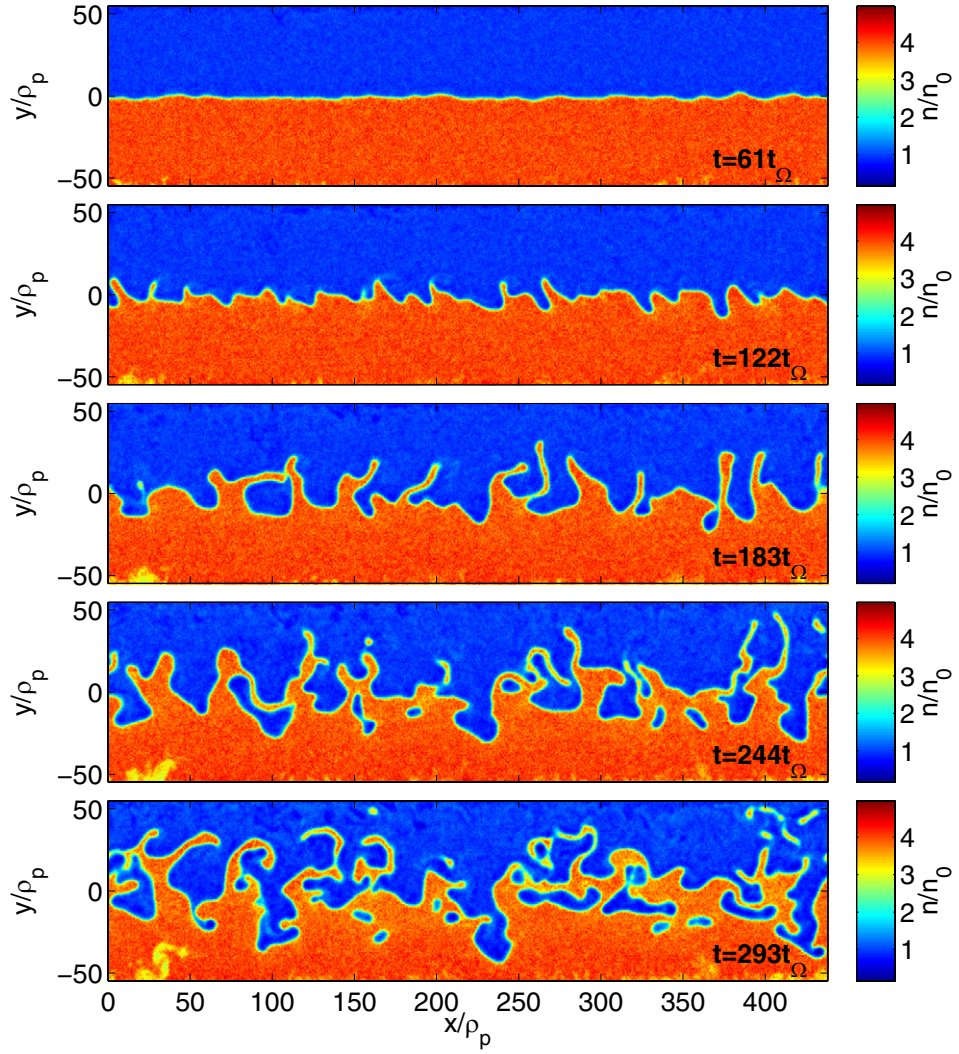

Figure 2. Total number density of ions for a simulation initialized with a pressure gradient of width $a = \Delta y$ at $y = 0$, and $n_{\text{bot}} = 5n_{\text{top}}$. Perturbations on the boundary layer visible from $t = 61t_\Omega$ are seen to grow at later times as a result of the interchange instability. The separation of blobs from the higher density layer begins at approximately $t = 200t_\Omega$.

simulations is shown for a proton plasma in figure 3 and for a D–T plasma in figure 4. From $60t_\Omega$ in the proton plasma case and $20t_\Omega$ in the D–T plasma case, we see the formation and growth of vortices along the boundary layer with growth rate inversely proportional to the scale size, characteristic of the K–H instability [25]. In both cases, separation of blobs occurs at the crests of the vortices generated by the K–H instability, and at earlier times relative to the simulation with zero velocity shear. The differences between the distribution of blob sizes created by the K–H and interchange instabilities will be discussed in the following section.

3.2. Structure statistics

Blobs play a significant role in particle and energy transport across the separatrix, which defines the LCFS of a tokamak plasma. However the distribution of blob sizes in the core-edge and SOL regions of tokamaks is not well known, particularly for scale sizes on the order of the ion gyro-radius. It is important to understand how significant kinetic effects are to the population as a whole, in addition to the phenomenology at individual blob level addressed in previous publications [19, 21]. Hence we now determine the distribution of blob sizes which develops as a result of the mechanisms represented in these simulations.

To obtain the statistics of blob structure sizes, we need a threshold condition to distinguish structures from the background. This is implemented across the spatial simulation domain (x, y) in terms of a conditional function $f(x, y, t)$; for example, in the case of over-dense blobs,

$$f(x, y, t) = \begin{cases} 1, & \text{if } n(x, y, t) > n_{\text{threshold}}, \\ 0, & \text{otherwise.} \end{cases} \tag{3}$$

We then define the connected regions in configuration space (x, y) for which $f(x, y, t) = 1$ to constitute a blob, and measure the properties of these regions, such as their area, to see how their statistics change with time.

We present size statistics for each simulation in terms of cumulative distribution functions $C(r) = \int_0^r P(r')\,\mathrm{d}r'$, where $P(r)$ is the distribution of blobs as a function of their radii,

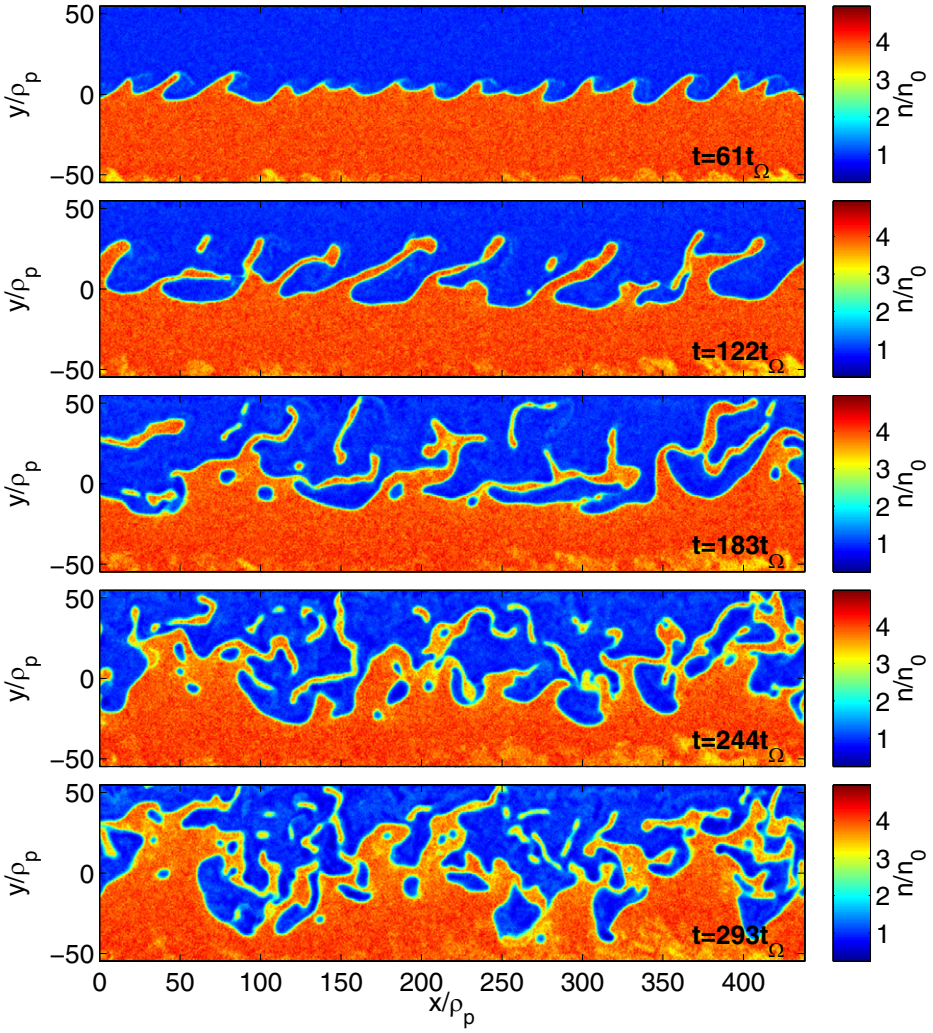

Figure 3. Total number density of ions for a proton plasma simulation initialized with a velocity shear boundary and pressure gradient at $y = 0$ with flows $u_{\mathrm{top/bot}} = \pm 0.02 v_{\mathrm{A}}$ and boundary width $a = \Delta y$. The combination of K–H and interchange instabilities leads to separation of blobs from the high-density, lower layer at significantly earlier times than the case with no shear boundary.

and in terms of rank order plots. The latter order blobs by radii from largest to smallest, and correspond to the inverse of $C(r)$ weighted by the total number of blobs. Cumulative distribution functions and rank order plots of blobs sizes are shown in figure 5 for the proton plasma simulation initialized with zero velocity shear. Simulations initialized with a velocity shear boundary are shown in figure 6 for the proton plasma case, and in figure 7 for the D–T plasma case. The minimum measurable blob size, limited by the size of the grid cells, is $0.4\rho_{\mathrm{p}}$.

These simulations demonstrate that ion gyro-scale blobs constitute a significant portion of the population of blobs in all scenarios discussed here. Approximately 70% of the blob population have radii less than $5\rho_{\mathrm{p}}$ in each scenario, with 10–30% having radii less than $2\rho_{\mathrm{p}}$.

We note several trends between simulations. First, once the interchange and K–H instabilities are sufficiently advanced to generate blobs, the cumulative distribution function of blob sizes tends to a distribution which is constant in time, i.e. it tends towards a saturated state. This is demonstrated most clearly by the distribution functions for the proton plasma case in figure 6, for which significant blob creation begins at $\sim 160 t_{\Omega}$. However, since blob creation is a rare event, significantly larger simulations are needed to confirm saturation in the tail of the distributions. Second, the inclusion of shear appears to lead to the creation of relatively fewer small-scale blobs. For example, with the inclusion of the shear boundary, the distribution function in figure 6 shows a sharp reduction in the number of blobs that have radii smaller than $4\rho_{\mathrm{p}}$, in contrast to the more uniform distribution in figure 5. A fit of the cumulative distribution functions to power laws at late times also demonstrates this reduction in the number of smaller blobs, with a corresponding increase in the power law exponent from $\alpha \sim 1.6$ in the zero-shear case to $\alpha \sim 2$. Finally, for D–T plasmas, the increase in ion gyro-radius at given particle energy, and inclusion of two ion populations with different gyro-radii, lead to an increase of the fraction of blobs at small scales. The sharp cut-off in the distribution function for blobs with radii less than $4\rho_{\mathrm{p}}$ in figure 6 is not observed for the D–T plasma case in figure 7, and the power law exponent at late times is reduced to $\alpha \sim 0.75$.

Previous studies [21] have shown that ion gyro-scale blobs are responsible for disproportionately more dissipation

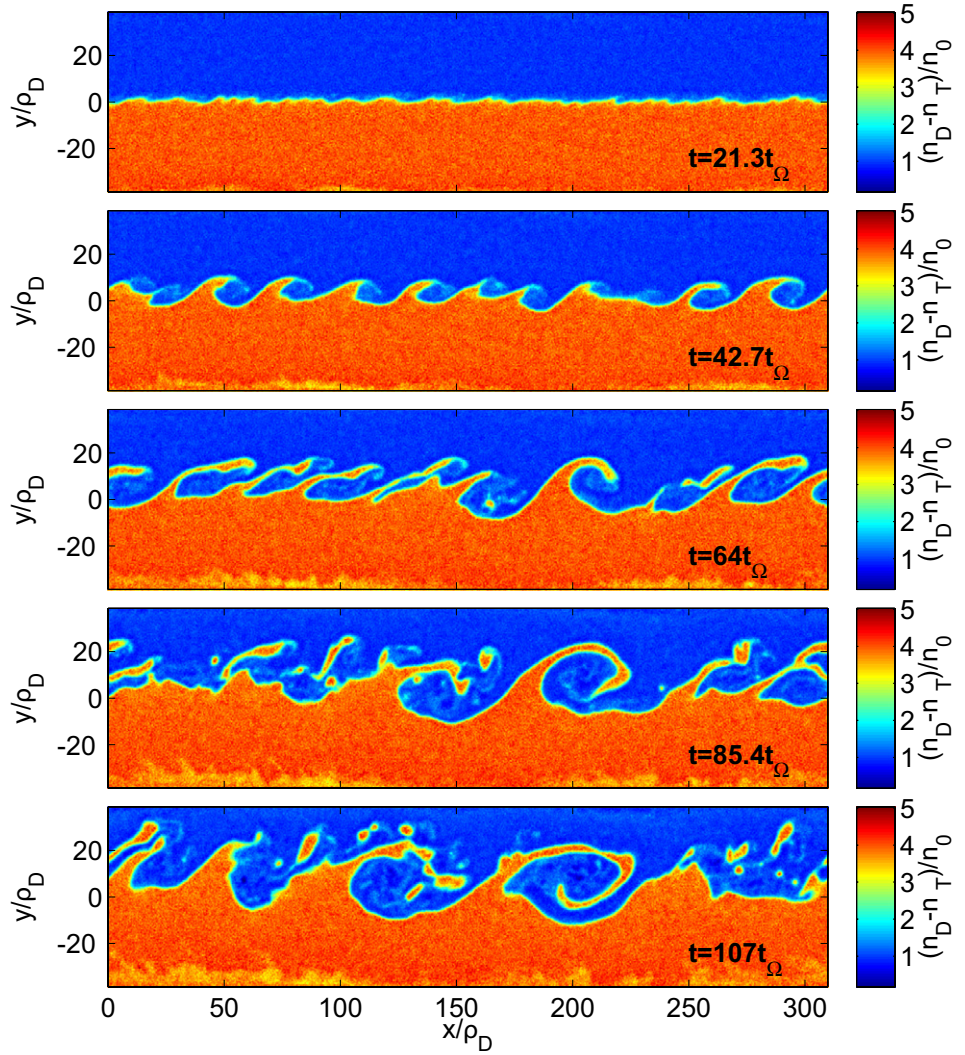

Figure 4. Total number density of all ion species for a D–T plasma simulation initialized with a velocity shear boundary and pressure gradient at $y = 0$ with flows $u_{\mathrm{top/bot}} = \pm 0.02 v_{\mathrm{A}}$ and boundary width $a = \Delta y$. The growth rate of both K–H and interchange instabilities is significantly reduced compared with the proton plasma cases, with suppression of small-scale modes. As a consequence, separation of blobs occurs at later times.

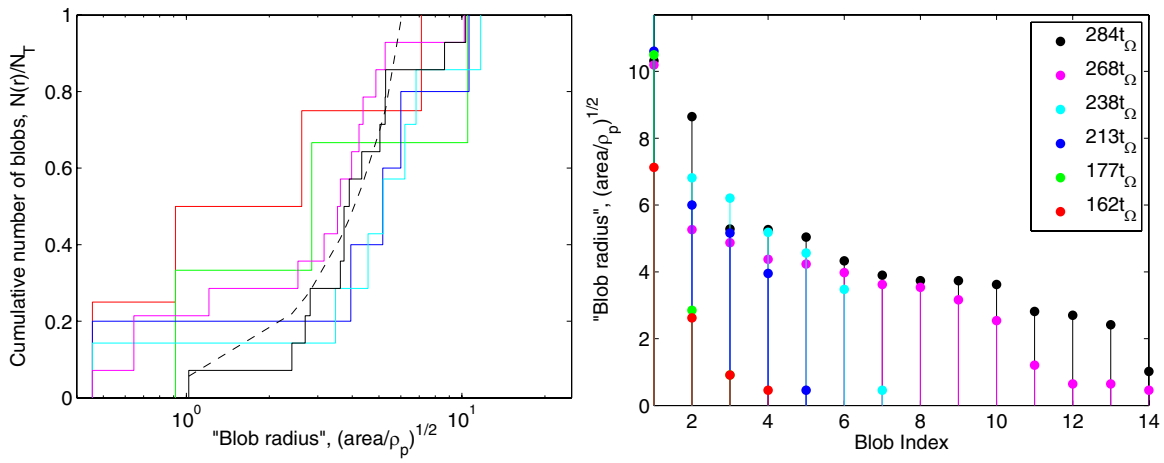

Figure 5. Cumulative distribution functions (left) and rank order plots (right) displaying the evolution of the distribution of blob sizes for a proton plasma simulation with a density gradient initialized at $y = 0$. A dashed line in the cumulative distribution function plot represents a power law $C(r) \propto r^{\alpha}$ with $\alpha = 2$.

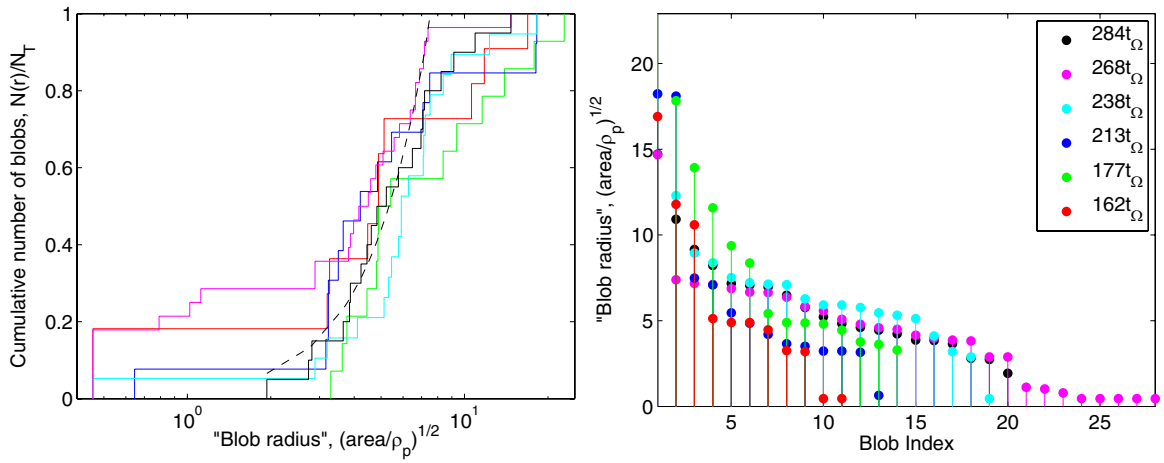

Figure 6. Cumulative distribution functions (left) and rank order plots (right) displaying the evolution of the distribution of blob sizes for a proton plasma simulation with a density gradient and velocity shear boundary initialized at $y = 0$. There is a steep increase in the relative number of blobs with radii above approximately $4\rho_p$. A dashed line in the cumulative distribution function plot represents a power law $C(r) \propto r^{\alpha}$ with $\alpha = 1.6$.

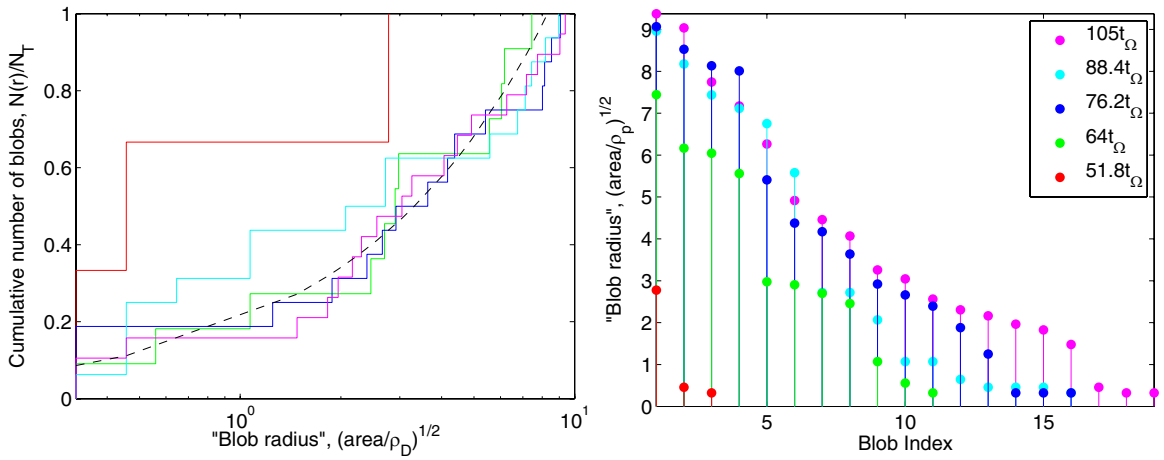

Figure 7. Cumulative distribution functions (left) and rank order plots (right) displaying the evolution of the distribution of blob sizes for a D–T plasma simulation with a density gradient and velocity shear boundary initialized at $y = 0$. A dashed line in the cumulative distribution function plot represents a power law $C(r) \propto r^{\alpha}$ with $\alpha = 0.75$.

of energy than larger, fluid-scale blobs. From the results presented in this section, we can further conclude that a significant population of ion gyro-scale blobs can exist in the near-edge region of a tokamak plasma. In combination, these conclusions reinforce the potential significance of the role of ion gyro-scale blobs for particle and energy transport in the edge region, including inside the SOL.

3.3. Particle diffusion

To characterize radial particle flux across the shear boundary, we calculate the mean square displacement $\langle \Delta y^2 \rangle$ for populations of ions initialized at regular spacing along $y = 0$, in the vicinity of the velocity shear boundary and density gradient. To characterize the time evolution of this mean square displacement, we define a diffusion coefficient D:

$$D = \frac{\langle \Delta y^2 \rangle}{t}. \tag{4}$$

We test for a power law increase in displacement such that $\langle \Delta y^2 \rangle \propto (\Omega_i t)^{\gamma}$. For classical diffusion, $\gamma = 1$ and the diffusion coefficient D is constant.

The dependence of the diffusion coefficient D and power law exponent γ on finite Larmor radius effects has been studied for turbulence in the edge region using both Hasegawa–Mima [27–30] and Hasegawa–Wakatani [31] reduced fluid models. Particle transport studies have included models of ion kinetics that are gyro-averaged [32, 33] or full Lorentz trajectories [34]. These simulations show that the effect of finite Larmor radius on particle transport is highly dependent on turbulent vortex scale sizes and shear boundaries. High frequency gyration effectively smooths out small turbulent fluctuations and leads to a reduction in transport [28, 30]. However, the reduction is less dramatic, and transport may even increase with gyro-radius, for slowly varying turbulent fluctuations on the order of the gyro-radius [31, 33, 34]. These studies typically report subdiffusive power law exponents $\gamma \sim 0$–1 in the radial direction, and superdiffusive power law exponents $\gamma \sim 1$–2 in the poloidal direction. However, in contrast to

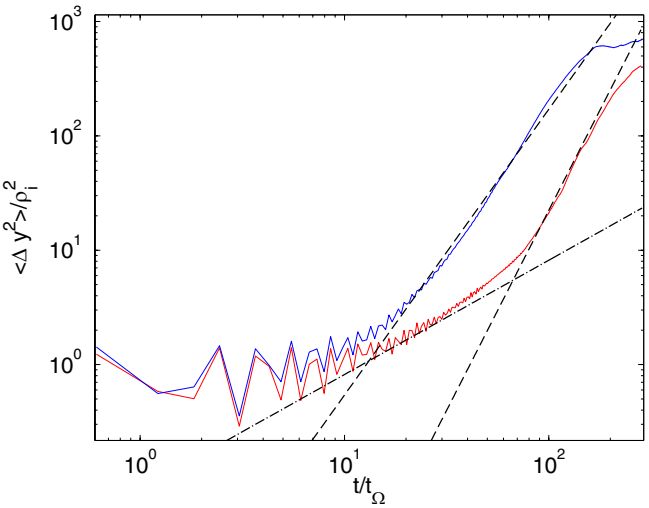

Figure 8. Mean particle displacement $\langle \Delta y^2 \rangle$ for proton plasma simulations initialized with a density gradient (red) and with both a density gradient and a velocity shear boundary (blue). Dashed lines display power laws with exponents $\gamma = 3.5$ overlaid on the red line representing the case of interchange only, and $\gamma = 2.5$ overlaid on the blue line representing the case of combined interchange and K–H instabilities. A dashed–dotted line displaying the standard diffusive power law $\gamma = 1$ is also given for comparison. Here we find that diffusion of particles is suppressed by the K–H dynamics associated with the shear boundary.

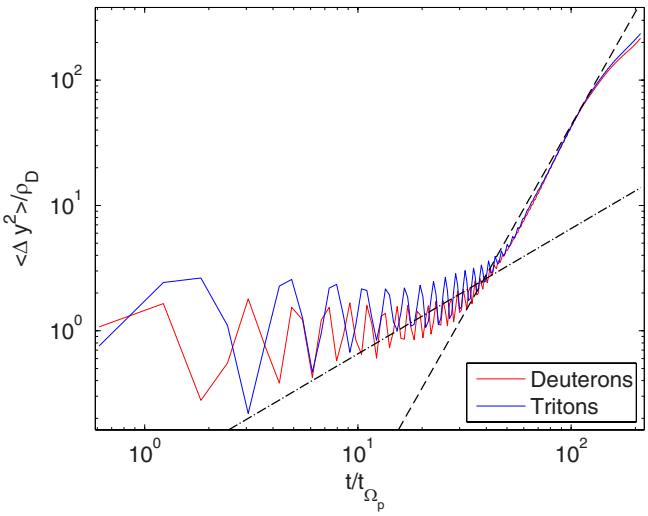

Figure 9. Mean particle displacement $\langle \Delta y^2 \rangle$ for a D–T plasma simulation including both pressure gradient and velocity shear boundary. A dashed line displays the power law with exponent $\gamma = 3$. Both deuterons and tritons follow this power law closely. A dashed–dotted line representing the standard diffusive power law $\gamma = 1$ is shown for comparison.

the geometry chosen here, these simulations include multiple shear layers at the boundaries of several zonal flows. Similar analyses have also been conducted for particle displacement by K–H and interchange instabilities at the magnetopause [35]. The geometry used in [35] more closely resembles the geometry chosen here, with resulting hyperdiffusive power law exponents $\gamma \sim 3$–4.

The calculated radial particle diffusion is plotted for proton plasma simulations with and without a velocity shear boundary in figure 8, and for a D–T plasma simulation with a velocity shear boundary in figure 9. A summary of the results is given in table 2. We find the greatest particle displacement occurs for the proton plasma simulation initialized without a shear boundary, with hyperdiffusive power law exponent $\gamma \sim 3.5$. With the introduction of a velocity shear boundary, the power law exponent is reduced to $\gamma \sim 2.5$, so we conclude that a shear boundary can reduce particle transport over long times. The reduction in transport by the shear boundary is a consequence of the trapping of particles within vortices generated by the K–H instability [31, 34]. As part of the dynamics of the K–H instability, these vortices fold up and coalesce at the boundary layer, and do not propagate radially. Particles trapped within these vortices therefore undergo reduced radial transport. In the D–T plasma case, we find that mean particle displacement is increased over the proton plasma case, and that deuteron and triton populations follow the same power law, with exponent $\gamma \sim 3$. These power law exponents are consistent with those measured for magnetospheric instabilities of similar geometry in [35], for which $\gamma \sim 3$–4. We note that this hyperdiffusive transport of particles initialized in the boundary region, which are representative of the population of ions in the propagating coherent structures, precedes the non-diffusive transport of blobs which cross the separatrix, as described in [4].

Table 2. Particle displacement power laws for simulations presented in this paper.

Ion species	Shear, $(u_{\text{top}} - u_{\text{bot}})/v_A$	Power law exponent, γ
Protons	0	3.5
Protons	0.04	2.5
D–T	0.04	3

4. Conclusions

These hybrid simulations show that radially propagating ion gyro-scale plasma blobs can be created via the interchange instability alone and in combination with the Kelvin–Helmholtz instability. The evolution of the boundary between plasma regions demonstrates that generation of these density blobs need not alter the magnetic topology of the plasma. Analysis of the distribution of sizes of blobs created by these instabilities shows that, for ion gyro-scale boundary widths, ion gyro-scale blobs can account for as much as 70% of the blob population. The introduction of a velocity shear boundary can increase the proportion of ion gyro-scale blobs, with the introduction of a cut-off in the distribution function of blob sizes. By comparing the statistics of blob creation between proton and D–T plasmas, we have found that an increase of the ion gyro-radius results in an increase of the fraction of blobs at smaller scales.

Analysis of the mean square displacement of particles demonstrates that the ion kinetic interchange and Kelvin–Helmholtz instabilities lead to hyperdiffusion of particles in the radial direction, with diffusion power law exponent $\gamma \sim 2$–4. We have shown that the introduction of a shear flow reduces the power law exponent, replicating experimental observations.

Hence, we infer that in the presence of shear, particles are less able to propagate into the tokamak SOL and interact with the vessel wall. Our D–T plasma simulations show that an increase in the ion gyro-radius relative to the boundary width results in an increase in particle transport in the radial direction.

In previous studies, we have examined how ion gyro-scale plasma blobs evolve [19], and demonstrated that they dissipate [21] disproportionately more energy than larger, fluid-scale blobs. Here we have investigated the physical processes by which ion gyro-scale blobs come in existence. This has led to the conclusion that ion gyro-scale blobs may constitute a significant portion of the blob population created inside the SOL, and that ion kinetic physics plays an important role in blob creation and particle transport. It follows that ion gyro-scale blobs are likely to be significant for the transport of particles and energy in the edge region of low-field tokamaks. Although this population cannot yet be resolved in experiments, its potential role in the energy budget of tokamak edge plasma is evident.

Acknowledgments

This work was part-funded by the EPSRC and the RCUK Energy Programme under grant EP/I501045 and the European Communities under the contract of Association between EURATOM and CCFE. The views and opinions expressed herein do not necessarily reflect those of the European Commission. PWG acknowledges support from the University of Warwick-Queen Mary University of London research partnership. We also thank the EPOCH development team for their work on the PIC code adapted for this research.

References

[1] Nedospasov A V 1992 *J. Nucl. Mater.* **196** 90
[2] Pedrosa M A *et al* 1999 *Phys. Rev. Lett.* **82** 3621
[3] Zweben S J, Boedo J A, Grulke O, Hidalgo C, La Bombard B, Maqueda R J, Scarin P and Terry J L 2007 *Plasma Phys. Control. Fusion* **49** 1
[4] Krasheninnikov S I 2001 *Phys. Lett.* A **283** 368
[5] Boedo J A *et al* 2001 *Phys. Plasmas* **8** 4826
[6] Grulke O, Terry J L, Labombard B and Zweben S J 2006 *Phys. Plasmas* **13** 012306
[7] Myra J R, D'Ippolito D A, Stotler D P, Zweben S J, Leblanc B P, Menard J E, Maqueda R J and Boedo J 2006 *Phys. Plasmas* **13** 092509
[8] Nold B, Conway G D, Happel T, Müller H W, Rohde V, Stroth U and the ASDEX Upgrade Team 2010 *Plasma Phys. Control. Fusion* **52** 065005
[9] Kirk A *et al* 2006 *Plasma Phys. Control. Fusion* **48** B433
[10] Kukushkin A S, Pacher H D, Pacher G W, Janeschitz G, Coster D, Loarte A and Reiter D 2003 *Nucl. Fusion* **43** 716
[11] D'Ippolito D A, Myra J R and Zweben S J 2011 *Phys. Plasmas* **18** 060501
[12] Russell D A, Myra J R and D'Ippolito D A 2007 *Phys. Plasmas* **14** 102307
[13] Bisai N, Das A, Deshpande R, Jha R, Kaw P, Sen A and Singh R 2005 *Phys. Plasmas* **12** 072520
[14] Terry J L *et al* 2005 *Nucl. Fusion* **45** 1321
[15] Cheng J *et al* 2010 *Plasma Phys. Control. Fusion* **52** 055003
[16] Myra J R *et al* 2011 *Phys. Plasmas* **18** 012305
[17] Xu G S *et al* 2009 *Nucl. Fusion* **49** 092002
[18] Furno I *et al* 2008 *Phys. Plasmas* **15** 055903
[19] Gingell P W, Chapman S C, Dendy R O and Brady C S 2012 *Plasma Phys. Control. Fusion* **54** 065005
[20] Madsen J, Garcia O E, Stærk Larsen J, Naulin V, Nielsen A H and Rasmussen J J 2011 *Phys. Plasmas* **18** 112504
[21] Gingell P W, Chapman S C and Dendy R O 2013 *Plasma Phys. Control. Fusion* **55** 055010
[22] Smolyakov A I, Diamond P H and Malkov M 2000 *Phys. Rev. Lett.* **84** 491
[23] Winske D, Yin L, Omidi N, Karimabadi H and Quest K 2003 *Space Plasma Simulation* (*Lecture Notes in Physics* vol 615) (Berlin: Springer) p 136
[24] Jun B-I, Norman M L and Stone, J M 1995 *Astrophys. J.* **453** 332
[25] Miura A 1984 *J. Geophys. Res.* **89** 801
[26] Hewett D W 1994 *Computer Phys. Commun.* **84** 243
[27] Manfredi G and Dendy R O 1996 *Phys. Rev. Lett.* **76** 4360
[28] Manfredi G and Dendy R O 1997 *Phys. Plasmas* **4** 628
[29] Annibaldi S V, Manfredi G, Dendy R O and Drury O'C 2000 *Plasma Phys. Control. Fusion* **42** L13
[30] Annibaldi S V, Manfredi G and Dendy R O 2002 *Phys. Plasmas* **9** 791
[31] Dewhurst J M, Hnat B and Dendy R O 2010 *Plasma Phys. Control. Fusion* **52** 025004
[32] Hauff T and Jenko F 2006 *Phys. Plasmas* **13** 102309
[33] Hauff T and Jenko F 2007 *Phys. Plasmas* **14** 092301
[34] Vlad M and Spineanu F 2005 *Plasma Phys. Control. Fusion* **47** 281
[35] Cowee M M, Winske D and Gary S P 2009 *J. Geophys. Res. (Space Phys.)* **114** A10209